X-RAY EMISSION FROM THE BASE OF A CURRENT SHEET IN THE WAKE OF A CORONAL MASS EJECTION

P. SAINT-HILAIRE, S. KRUCKER, AND R.P. LIN

Space Sciences Laboratory, University of California, Berkeley, CA 94720, USA; shilaire@ssl.berkeley.edu

ABSTRACT

Following a coronal mass ejection (CME) which started on 2002 November 26, *RHESSI* observed for 12 hr an X-ray source above the solar limb, at altitudes between 0.1 and 0.3 R_S above the photosphere. The *Geostationary Operational Environmental Satellite* baseline was remarkably high throughout this event. The X-ray source's temperature peaked around 10–11 MK, and its emission measure increased throughout this time interval. Higher up, at 0.7 R_S, hot (initially >8 MK) plasma has been observed by Ultraviolet Coronograph Spectrometer on *Solar and Heliospheric Observatory* for 2.3 days. This hot plasma was interpreted as the signature of a current sheet (CS) trailing the CME. The thermal energy content of the X-ray source is more than an order of magnitude larger than in the CS. Hence, it could be the source of the hot plasma in the CS, although CS heating by magnetic reconnection within it cannot be discounted. To better characterize the X-ray spectrum, we have used novel techniques (back-projection-based and visibility-based) for long-integration (several hours) imaging spectroscopy. There is no observed nonthermal hard X-ray bremsstrahlung emission, leading to the conclusion that there is either very little particle acceleration occurring in the vicinity of this postflare X-ray source, or that either the photon spectral index would have had to be uncharacteristically (in flare parlance) high ($\gamma \gtrsim 8$) and/or the low-energy cutoff very low ($E_c \lesssim 6$ keV).

Key words: Sun: flares – Sun: particle emission – Sun: X-rays, gamma rays

Online-only material: color figures

1. INTRODUCTION

During solar flares, particles are believed to be accelerated, and plasma heated as a result of magnetic reconnection at an X-point or neutral sheet in the corona (Kopp & Pneuman 1976). The accelerated electrons stream down to the footpoints of coronal magnetic loops, producing hard X-ray (HXR) bremsstrahlung as they are thermalized by Coulomb collisions in the dense lower corona or chromosphere. The directly heated plasma already in the loop and the ablated chromospheric material produce hot loops below the reconnection site, with temperature that can be 20 MK or higher, and densities as high as 10^{11} cm^{-3}. These loops are visible in soft X-rays, and later, as they cool down, become visible in EUV and in Hα. The reconnection site gradually moves upward and continues to release energy, even as the X-ray flux diminishes. This translates into the appearance of higher and higher hot loops, and cooler loops at the lower altitudes (see, e.g., Svestka 1987).

Coronal mass ejections (CMEs) are often associated with flares. One of the models invoked in their creation is the catastrophe or flux-rope model (see, e.g., Lin & Forbes 2000), in which a current sheet (CS) is thought to extend from the top of the reconnected loop system to the plasma bubble that surrounds the expelled flux rope. A CS is supposed to be so thin as to make direct observation quite difficult. However, there have recently been reports of CS detection in the extended corona from observations acquired in the wake of CMEs by the Ultraviolet Coronograph Spectrometer (UVCS; Kohl et al. 1995), in the form of narrow, very hot (several MK) features, most prominently in the Fe^{17+} line: Ciaravella et al. (2002), Ko et al. (2003), Raymond et al. (2003), Lin et al. (2005), Bemporad et al. (2006), Bemporad (2008), and Ciaravella & Raymond (2008). In particular, Ciaravella & Raymond (2008) have firmly established that the CS thickness (for one event, at

least) to be between 0.04 and 0.08 R_S, far larger than classical ($\lesssim$100 m) or anomalous (a few tens of km) resistivity would predict. In a re-analysis of previous results, Bemporad (2008) have explained these observations with the existence of many ($\sim10^{-11}$ to 10^{-17} m^{-3}) microscopic CSs of small sizes ($\approx$10–10^4 m) that, through nonthermal turbulent broadening, can justify not only the high CS temperatures but also the large observed thicknesses of macroscopic CSs.

Bemporad et al. (2006) examine one such event, which lasted at least 2.3 days. The CME to which these observations pertain started at around 17:00 UT on 2002 November 26 on the western limb of the Sun. Bemporad et al. (2006) discuss in detail UVCS, Large Angle and Spectrometric Coronograph (LASCO; Brueckner et al. 1995) and Extreme Ultraviolet Imaging Telescope (EIT; Delaboudinière et al. 1995; instruments on board *SOHO*, the *Solar and Heliospheric Observatory*) observations of this event. Our paper will concentrate on examining the concurrent X-ray emission, with data from *Geostationary Operational Environmental Satellite* (*GOES*), and *RHESSI* (Lin et al. 2002), which was launched a few months prior to this event.

Section 2 will briefly summarize the observations reported by Bemporad et al. (2006), then complement them with X-rays observations: light curves, spectra, and imaging. Section 3 will then discuss interpretations of these observations, and the possibility that accelerated nonthermal particles provide the energy required to power the X-ray source, and perhaps the CS.

2. OBSERVATIONS

2.1. Brief Summary of Previously Reported Observations

Bemporad et al. (2006) have reported observing a CS in the wake of a CME that started on 2002 November 26 around 17:00 UT. That conclusion was mainly supported by UVCS observations (starting at 18:39 UT) of a hot (initially well beyond
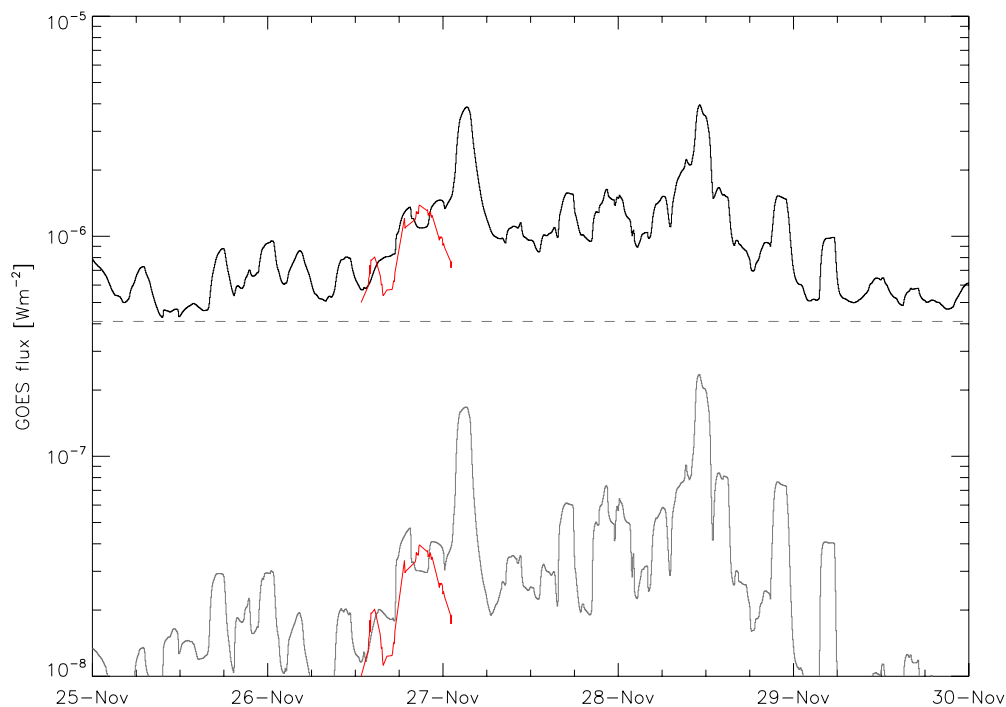
Figure 1. *GOES* light curves: black is the 1–8 Å flux, the gray line is the 0.5–4 Å flux. The data have been smoothed using a 2 hr smoothing window. The dashed line represents a constant flux at 4.1×10^{-7} W m^{-2}. The red line represents *RHESSI* 4–8 keV flux from the coronal source only.

(A color version of this figure is available in the online journal.)

8 MK) plasma above the western limb of the Sun ($\approx 25°$ north latitude), in the same radial direction as the CME, at an altitude of about 0.7 R_S above the solar photosphere, directly above a loop system observed with EIT. This hot plasma had a width of ≈ 100 Mm perpendicularly to the radial direction from the Sun and to our line of sight. It cooled to 3.5 MK after 2.3 days, at which point UVCS observations stopped.

Bemporad et al. (2006) also estimated that adiabatic heating is insufficient to explain the hot plasma, at least initially, and that reconnection must be the source of the thermal energy. In his re-analysis, Bemporad (2008) further strengthens that hypothesis.

The remainder of this section will concentrate on complementing the aforementioned study with X-ray observations from *RHESSI* and *GOES*.

2.2. X-ray Light Curves and Imaging

As can be seen in Figures 1 and 2, on 2002 November 26, around 13:40 UT, the *GOES* "baseline" in both channels increased suddenly, and stayed fairly high until 2002 November 29 $\approx$00:00 UT. During this time interval, several flares occurred at different positions on the solar disk, revealed as individual peaks in the *GOES* light curves (which are spatially integrated) of Figure 2.

At about 12:00 on November 26, a solar flare started (Figure 2, first and third plots). It was observed with *RHESSI* on the western limb of the Sun, at about 25° of north latitude. *RHESSI* observed it until $\approx$12:42, at which time it entered Earth's shadow. Very shortly (3–4 minutes) after the rise in *GOES* fluxes at $\approx$13:40, *RHESSI* came out of Earth's shadow, and imaged an X-ray source at the same solar latitude, but about 80 Mm above the limb (Figure 3). This high-altitude coronal X-ray source (hereafter HACXS) remains observable by *RHESSI* until $\approx$01:10 the next day (2002 November 27), i.e., for almost 12 hr. During that 12 hr period, several disk flares

occurred, and with their much higher fluxes, often drowned the HACXS when attempting imaging.

From its start at about 13:45, to about 16:00, the HACXS moved mostly radially outward from the Sun, at about 1.6 km s^{-1} (Figure 2). During that time, the HACXS flux increased and then decreased. At about 16:15, the source seemingly "jumps" in altitude, by about 60 Mm. It could be argued that our initial source actually dimmed, and that this is a new, different source that appears at higher altitude. The *RHESSI* coverage between $\approx$16:00 and $\approx$17:00 is spotty: during that time interval, a flare occurred on the eastern limb of the Sun (introducing noise in images of our region of interest (ROI)), the spacecraft was initially in the South Atlantic Anomaly (with detectors turned off), and also spent time in Earth's shadow. The 5 minute image that shows a source midway between the two sites (at $\approx$16:20 in Figure 2) suggest we might indeed have had a single exciter that jumped across 60 Mm in about 70 minutes ($\approx$14 km s^{-1} velocity).

Between about 16:00 and 18:45, the X-ray source moved progressively faster toward the solar equator (azimuthal velocity close to 5 km s^{-1}), then stopped just as a flare at the footpoint of the loop system appears (position [900, 400] in Figure 3). EIT images show the rise of a filament-like feature at around 16:12, from the same active region, and a cusp-like feature and expelled material at around 17:12–17:24, the latter two in the same direction as the CME, starting below the HACXS altitude, and just a few tens of arcseconds northward of it.[1]

The X-ray source then settled on a mostly radial course at $\approx$2 km s^{-1}, before ceasing to be observed by *RHESSI* around 01:10 on 2002 November 27. This velocity is in very good agreement with the velocity of the rising post-CME loop systems observed with EIT (Figure 2). The HACXS stays well above ($\sim$0.1 R_S) the EUV loop system throughout the observations.

---

[1] http://sprg.ssl.berkeley.edu/~shilaire/movies/20021126_js/
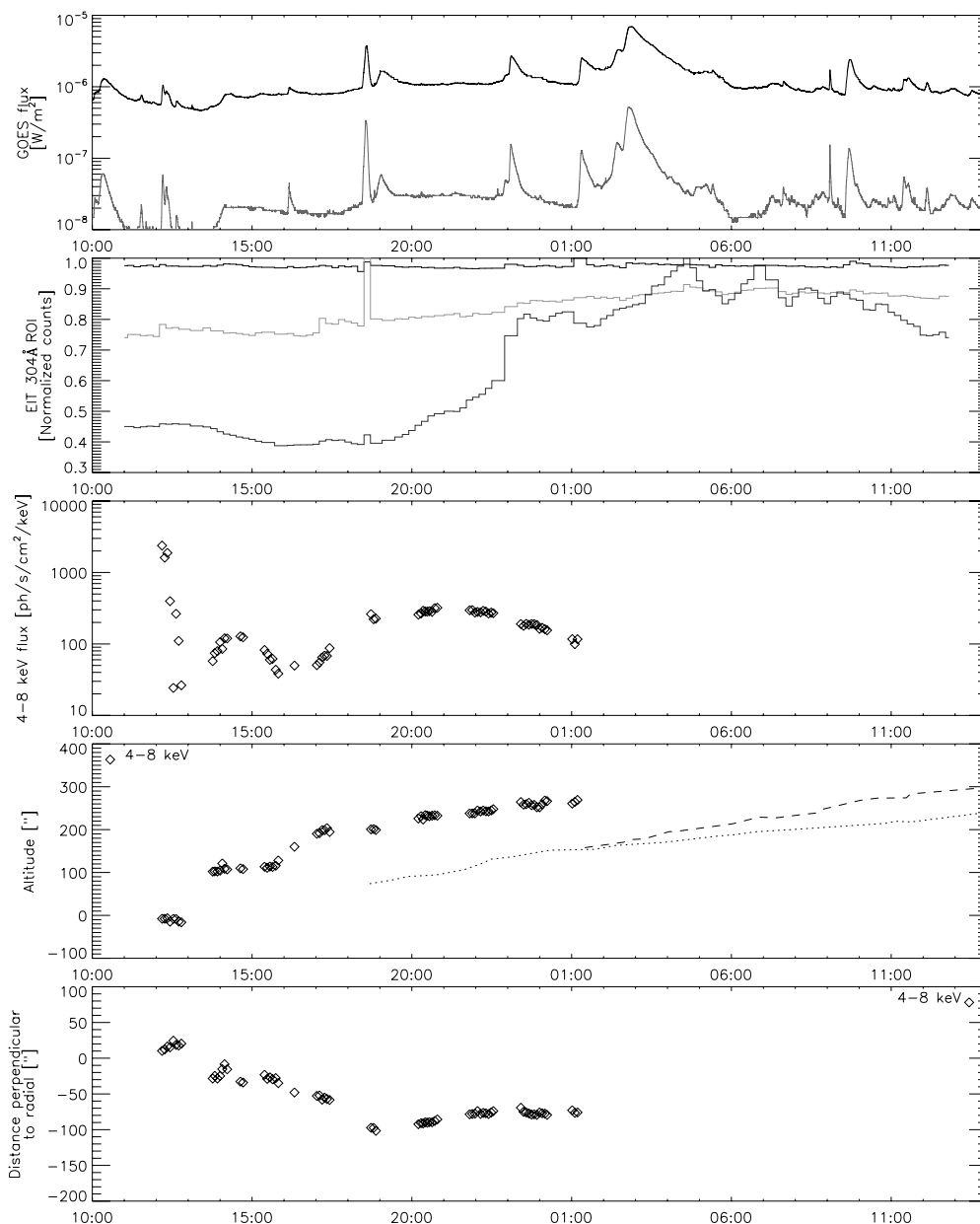
Figure 2. First (top) plot: *GOES* light curves (black: 1–8 Å, gray: 0.5–4 Å). Second plot: EIT light curves (black: full Sun, light gray: ROI is 600″ square centered around [1050, 450], i.e., encompassing slightly more than Figure 3, dark gray: ROI is 200″ × 300″ rectangle centered at [1050, 450]), shown as a green box in Figure 3. Third plot: *RHESSI* 4–8 keV flux from imaging with ROI being a 256″ square centered around [1100, 400]. Fourth plot: diamonds: source altitude in the 4–8 keV band, from *RHESSI* imaging using subcollimator 8. Dashed line: northern EIT loop system altitude (from Bemporad et al. 2006). Dotted line: southern EIT loop system altitude (from Bemporad et al. 2006). Fifth plot: source azimuthal distance from an arbitrary radial, using *RHESSI*'s subcollimator 8 in the 4–8 keV band. In the *RHESSI* plots (last three plots), the displayed information includes the initial flare at ≈12:00 UT. Beyond 13:00 UT, the plots only display the information pertaining to the coronal source, removing any disk flares.

2.2.1. X-ray Source Size and Shape

Using *RHESSI* visibilities (a new software method akin to radio visibilities, see, e.g., Schmahl & Hurford 2003), source size, shape, and position were determined and are displayed in Figure 4 at different energies. Higher energies tend to be at higher altitude, suggesting that the hottest plasma is at higher altitude, as would be expected if the reconnection X-point already flew past our ROI (see Section 3 and Appendix A).

Source size does not vary remarkably during the 12 hr interval. The shape of the HACXS stays generally elongated, with the higher energies having the tendency for higher eccentricities.

2.2.2. Spectroscopy

Spectroscopy of our high-altitude X-ray source was done. In Figure 5, full-Sun spectroscopy (purple) was done using the OSPEX *Solarsoft* suite of routines. Background selection and subtraction is a delicate process, particularly for that event, as disk flares occurred during the 12 hr time interval that the HACXS was observed. Hence, imaging spectroscopy was also employed: it is less sensitive than full-Sun spectroscopy, but does provide the inherent ability of removing background effects. The best spectrum from imaging was obtained by making 5 minute long images over 5 hr (2002 November 26 20:10 to 2002 November 27 01:10 UT), adding them together (rebinning
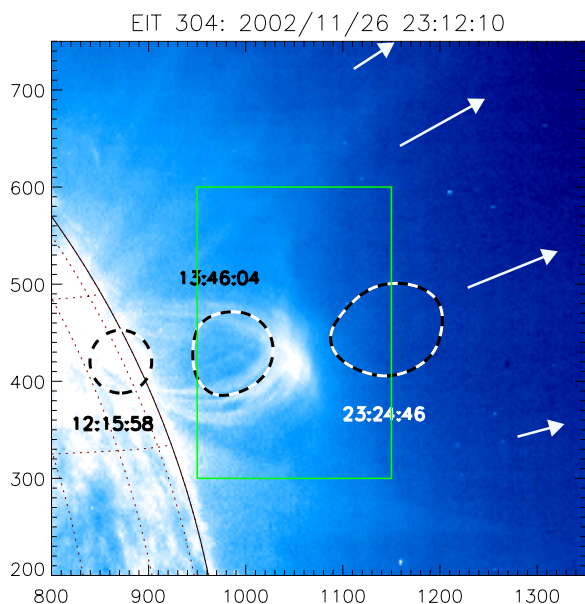
EIT 304: 2002/11/26 23:12:10

Figure 3. *SOHO*/EIT 304 Å image taken at 23:12:10 on 2002 November 26, with *RHESSI* 6–12 keV contours (50% level) at different times (5 minute exposures centered around 12:15:58, 13:46:04, and 23:24:46 UT). Using values from Figure 6 and from Figure 9 (top left) of Bemporad et al. (2006), we have drawn arrows that delimit the angular extend of the region where UVCS observed hot plasma at 1.7 R_S. The long arrows delimit the region of plasma above 5 MK, while the short arrows delimit plasma above 3 MK. The green box is the ROI used to compute the dark gray light curve in the second plot of Figure 2.

(A color version of this figure is available in the online journal.)

and shifting for source motion), and determining fluxes at different energies (i.e., spectrum) using back-projected maps with subcollimator 8 (Hurford et al. 2002): the noise level is typically four times smaller than from a spectrum obtained by simply adding together the spectra from each 5 minute accumulations. As an additional check, visibility-based imaging spectroscopy was also employed: the visibilities were phase-shifted to remove smearing from the source motion over 5 hr. The results are displayed as green data points in Figure 5, and a long-integration image of our event is shown in Figure 6. The spectra display no clear nonthermal (power-law) emission at high energies.

Fitting an isothermal component below 15 keV to the 5 hr back-projected data (blue data points in Figure 5) yield a temperature of $T = 11.4$ MK and emission measure EM $= 1.4 \times 10^{47}$ cm^{-3}. For comparison, 5 minutes long accumulation on 2002 November 26 around 20:30 UT yields $T = 11.5$ MK and 1.2×10^{47} cm^{-3} with imaging and $T = 9.5$ MK and 2.3×10^{47} cm^{-3} with spatially integrated spectroscopy (Figure 5, black and purple data points). The lower temperature and higher emission measures obtained from *RHESSI* full-Sun spectroscopy are probably due to the presence of a low-energy flux component with large spatial extend, the likely residuals from previous disk flares. The even lower temperatures and higher emission measures measured by *GOES* ($T = 7.5$ MK, EM $= 10^{48}$ cm^{-3}) at the same time and throughout this event (Figure 7) are typically attributed to the *GOES* response (see, e.g., Holman et al. 2003), which is more sensitive to lower temperature plasmas.

3. DISCUSSION

3.1. X-ray Source Timeline, Position, and Morphology

The HACXS first appeared some 80 Mm above the footpoints of a loop system, about 1.5 hr after a flare located in these

footpoints erupted. It progressed generally outward, its intensity rising and then decreasing over the course of ≈2 hr. From ≈17:00 to ≈19:30, EIT observed material being formed (e.g., a cusp feature and a filament feature) and expelled (e.g., a flux rope, and other ejecta). These ejections seem to have disturbed the HACXS: it jumped about 60 Mm in altitude, and its flux started increasing again.

The height and velocity profiles of the HACXS and the EUV loop system support the picture of a looptop (or "above the looptop") reconnection point that moves upward, heating the local plasma to X-ray-emitting temperatures, before they cool down and are later seen in EUV, giving the impression that the EUV loops trail the X-ray source in space, when in fact they are trailing in time. Apart from its very long duration, the source altitude profile of the HACXS is very similar to the observations reported by Gallagher et al. (2002), including the higher energies being located at slightly higher altitudes than the lower energies. This further supports the scenario that hotter plasma is located at higher altitude (see Appendix A for a simple justification, and Section 3.2 for an attempt at modeling it), consistent with the Kopp & Pneuman (1976) model and the Svestka (1987) observations.

After ≈21:00, the high-eccentricity (elongation) and orientation of the two-dimensional Gaussians fitted to the HACXS (as shown in the two bottom plots of Figure 4) are consistent with the geometry of a CS-like feature that extends radially outward.

The HACXS ceased to be observed by *RHESSI* around 01:10 UT on 2002 November 27. This is due to both it having decreased in intensity to near or below *RHESSI*'s sensitivity and the intense flaring activity that started at that time and lasted several hours. As observed in Figure 1, the *GOES* baseline (i.e., nonflaring level) after 2002 November 27 ≈01:10 UT is ill-determined, because of the intense flaring activity. But it is conceivable that the HACXS remains present until 2002 November 29 ≈00:00, as the *GOES* X-ray flux in both *GOES* channels never drops back to pre-event levels until then.

3.2. Energy–Position Relationship

The peak emissions at different energies are slightly displaced (Figure 4). In fact, Sui & Holman (2003) and Liu et al. (2008) have observed similar behavior with *RHESSI* X-ray data: they observed the centroid position of successively higher energies to be located at higher altitude, and, then the trend reversed. They have attributed this behavior to a hot CS located at the position where the trend reversed. Another possibility to explain the spatially displaced energies is the presence accelerated particles which, much as in Brown et al. (2002), are being stopped at larger distances (column densities) the larger their initial energies are. Although the greater elongation observed at high energies supports that scenario (see, e.g., Appendix A of Saint-Hilaire et al. 2009), the absence of nonthermal radiation (discussed in Section 3.3.2) in the spatially integrated spectrum clearly dispels that hypothesis.

We have considered different models of temperature and emission measure profiles (see Appendix A) to model the emission of different energies at different positions. We have attempted to fit our *RHESSI* data (visibilities accumulated from 2002/11/26 20:10 to 2002/11/27 01:10, and phase-shifted to remove source motion smearing) with the last two models mentioned in Appendix A: the first one, using exponential profiles (with altitude) for both temperature and emission measure, yielded very poor results. The second one, where the temperature profile was assumed Gaussian, and the emission measure
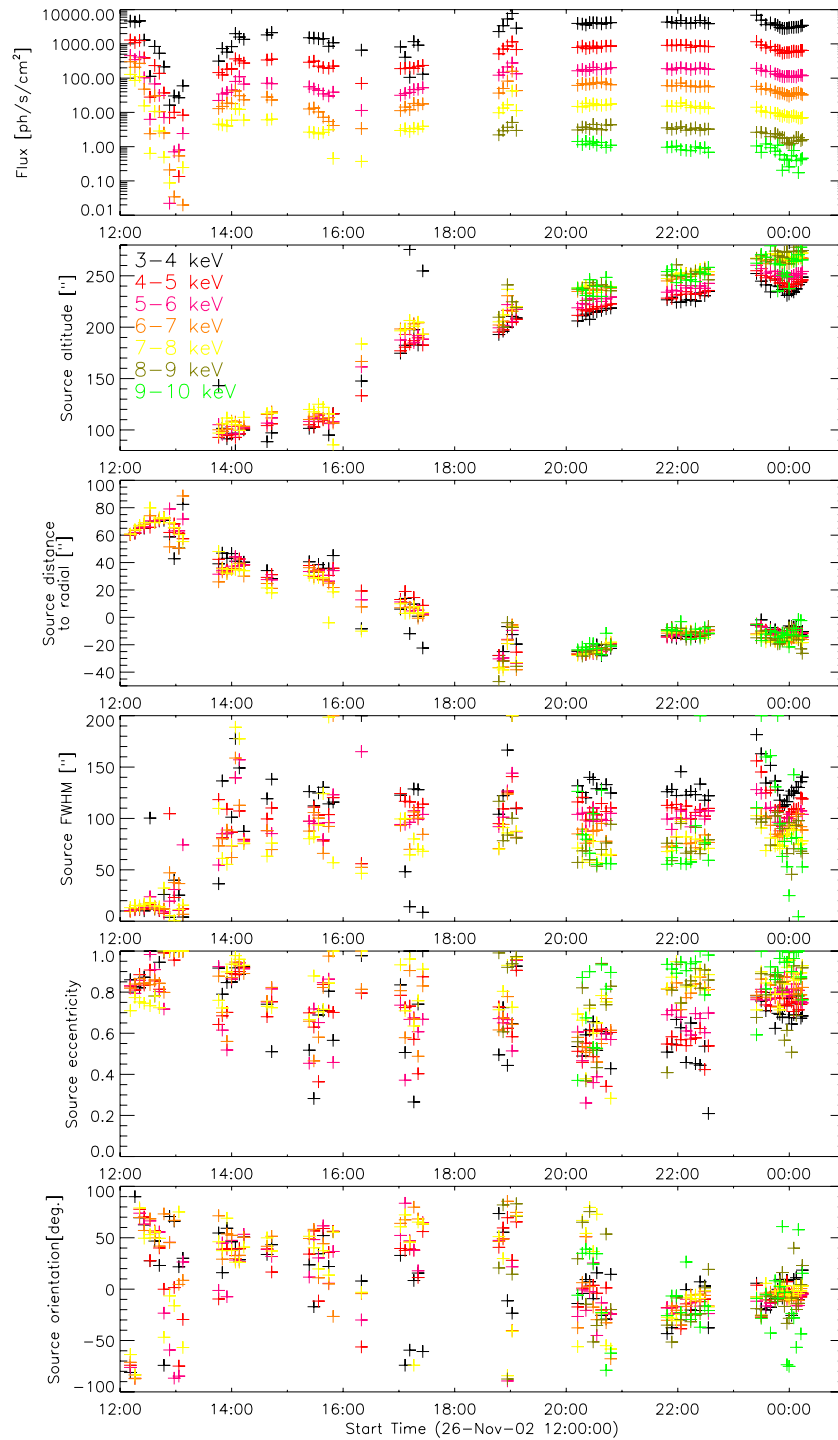
Figure 4. HACXS characteristics at different energies, derived from *RHESSI* visibilities accumulated over 5 minute intervals: flux, altitude above photosphere, distance to 25° radial; two-dimensional Gaussian FWHM, eccentricity, and orientation with respect to solar equator. For clarity, error bars were omitted, but the scatter of the points is a good approximation. Information on the 8–9 and 9–10 keV bands has been omitted before 18:00 and 20:00 UT, respectively, because of their weak fluxes. (A color version of this figure is available in the online journal.)

profile remained exponentially decreasing with altitude, yielded better results: the best-fitting parameters were $T_0 = 119$ MK, $H_T = 38''.1$, $H_{EM} = 657''$, $z_0 = 1221''.7$, and reduced $\chi^2 = 0.33$ (Figure 8, black). Such a high temperature seems highly unlikely. The synthetic X-ray spectrum computed from a plasma with such a temperature distribution (Figure 8, right) is clearly not observed. The height scales are loosely compatible with the typical density height scales found in the corona (about $100''$). Given that our error bars are rather large (partly explain-

ing the good χ^2 despite the obviously too-high temperature), we have tried for comparison to fix the temperature T at 10 MK, and redo the fitting process. We found $H_T = 4115''$, $H_{EM} = 64525''$, $z_0 = 1232''.8$, and reduced $\chi^2 = 0.9$ (Figure 8, gray). The corresponding synthetic spectrum is more in accordance with our observations, but these new rather large scales heights are somewhat unexpected, and would mean that the densities along the HACXS (and possibly the CS) change very slowly with altitude.
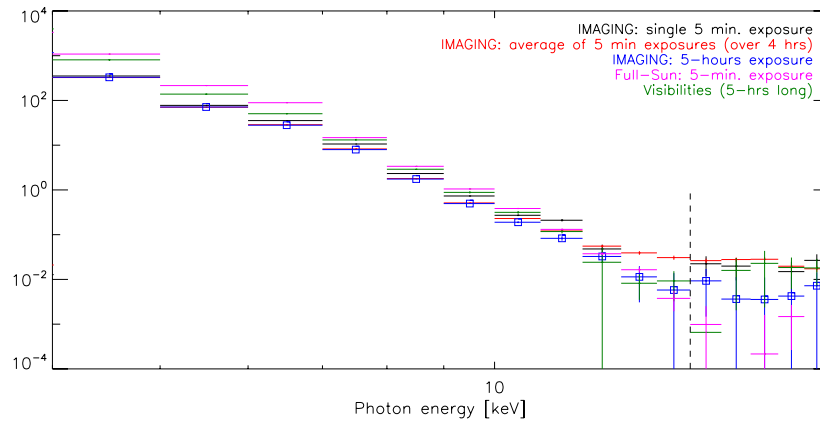
Figure 5. *RHESSI* spectra obtained using different methods. Black data points: *RHESSI* imaging spectroscopy with SC 8, accumulated between 2002/11/26 20:30:24 and 20:35:24 UT, with the vertical error bars. The horizontal error bars actually correspond to the bin widths. Red data points: average of all 5 minute imaging spectroscopy spectra (using SC 8) from 2002/11/26 20:00 to 24:00 UT. Blue data points: imaging spectroscopy with SC 8, using the sum of all 5 minute images between 2002/11/26 20:00 and 24:00 UT. Each image has been shifted in accordance with the source motion. Purple data points: spatially integrated spectroscopy between 2002/11/26 20:30:24 and 20:35:24 UT. Isothermal fitting yields 9.5 MK and 2.3×10^{47} cm^{-3}. Green data points: visibility derived (shifted phase centers) between 2002/11/26 20:10 and 2002/11/27 01:10 UT. Most methods yield unreliable values beyond ≈ 15 keV (black vertical dashed line), where background count rate is typically an order of magnitude above the source count rate.

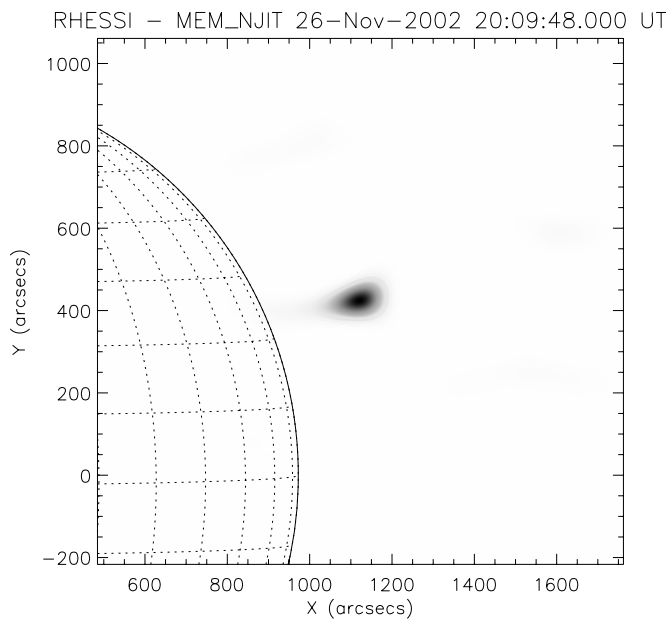(A color version of this figure is available in the online journal.)

Figure 6. Five-hour long *RHESSI* image, from 2002/11/26 20:10 to 2002/11/27 01:10 UT, in the 4–8 keV energy band. *RHESSI* visibilities were generated in 5 minute accumulations, then bundled together after shifting their phases to remove source motion effects (relative to the source position at 20:09:48 UT).

A full exploration of the model space and other fitting techniques are beyond the scope of this paper, but will be addressed in a subsequent one.

3.3. Energetics

3.3.1. Thermal Energy in RHESSI Source

We now want to estimate how much power and energy are needed to maintain the X-ray source at such high temperature for such a long time. On 2002 November 26, around 20:30, *RHESSI* observations indicate the source has an emission measure of about 2×10^{47} cm^{-3}, and a source size of $\approx 100''$ FWHM, leading to a source volume $V = 2 \times 10^{29}$ cm^3 (assuming that the HACXS has a spherical shape). Using $n = \sqrt{EM/V}$, one obtains an electron density $n = 10^9$ cm^{-3}, and a total number
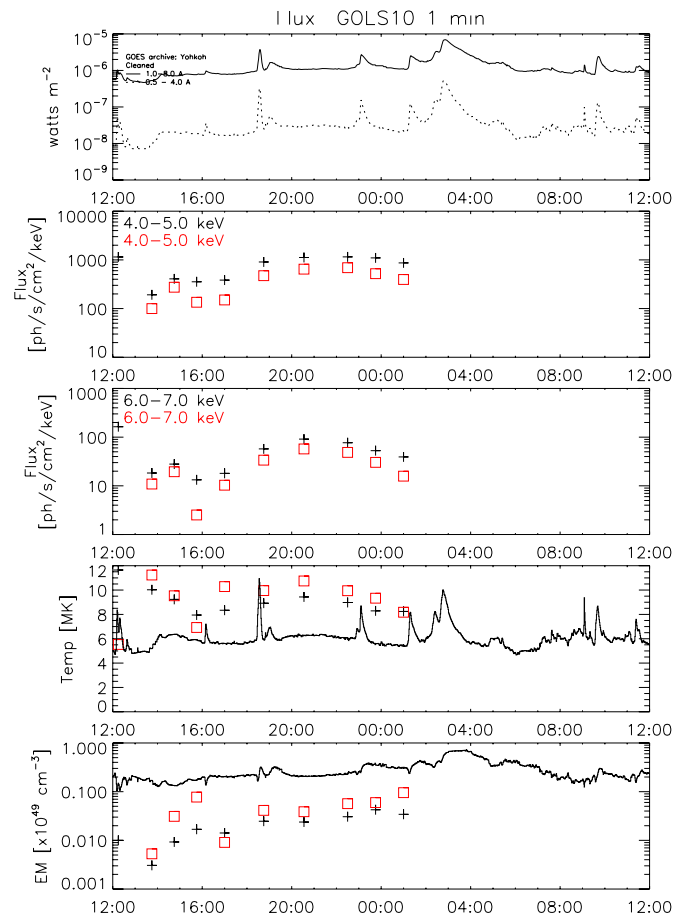

Figure 7. Black crosses: *RHESSI* full-Sun spectroscopy. Red squares: *RHESSI* imaging spectroscopy (SC 8). Solid black line: *GOES* temperature and emission measure measurements. The short duration (∼minutes) peaks observed by *GOES* are due to disk flares, unrelated to the HACXS.

(A color version of this figure is available in the online journal.)

of electrons $nV = 2 \times 10^{38}$ electrons (incidentally, a typical number for the total flare-accelerated electrons found in HXR footprints of large flares). With the temperature $T \approx 10.5$ MK (average of the 9.5 MK and 11.5 MK found in Section 2.2.2),
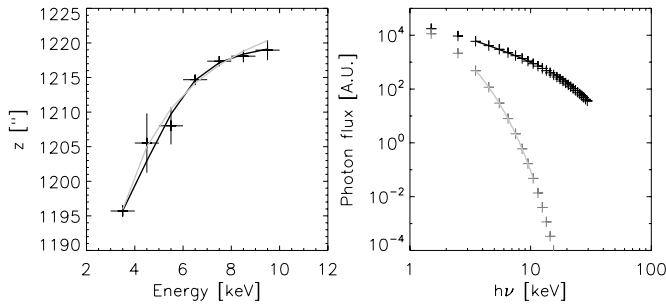
Figure 8. Left: crosses: positions of emission at different energies, with error bars (vertical lines) and bin widths (horizontal lines). Solid black line: fitting to the Gaussian T and exponential EM profiles. Solid gray line: same, with T fixed to 10 MK. Right: crosses: synthetic X-ray spectra generated using the fitting parameters found. Solid line: fit to the crosses in the 4–10 keV band. Color scheme same as in the plot on the left. See the text for more details.

this leads to a radiative loss timescale of $\tau_{\rm rad} \approx 8 \times 10^4$ s. The half loop length from the chromospheric footpoint to the HACXS is $L \approx \pi/2 \times H$, with the source height $H = 220''$, from which the conductive loss timescale $\tau_{\rm cond} \approx 8 \times 10^2$ s can be derived (see, e.g., Aschwanden 2004; we assumed that the energy is lost mainly to the chromospheric heat sink, and not to interplanetary space via open field lines). Conductive losses are more important than radiative losses, and we will hence use the former to estimate the power P required to maintain the temperature of the high-altitude X-ray source at around 10 MK, using

$$P = \frac{E_{\rm th}}{\tau_{\rm cond}} = \frac{3kTnV}{\tau_{\rm cond}}, \qquad (1)$$

$$\approx 6 \times 10^{35} \text{ keV s}^{-1} \approx 1 \times 10^{27} \text{ erg s}^{-1}, \qquad (2)$$

where k is Boltzmann's constant, and $E_{\rm th}$ is the thermal energy content of the source ($\approx 9 \times 10^{29}$ erg around 20:30 UT), i.e., over 12 hr, about 4×10^{31} erg must have been deposited in the source.

3.3.2. Nonthermal Energy

If the power P calculated in the previous paragraph came exclusively from accelerated particles as they dump all their energy into heating the plasma, could it be that their associated nonthermal emission is so weak as to be unobservable by *RHESSI*? A photon power law with spectral index $\gamma \approx 8$ and flux at 10 keV $F_{10} \approx 3 \times 10^{-2}$ photons s^{-1} cm^{-2} keV^{-1} is an order of magnitude below the observed (thermal) X-ray emission (Figure 5), and could be concealed by it. The characteristics of the electron distribution corresponding to such a hypothetical nonthermal photon emission can be determined assuming either *thick-target* or *thin-target* assumptions: the column density traversed $N = nL = 2.5 \times 10^{19}$ cm^{-2} stops injected electrons with start energy below 11 keV. $N = n\sqrt[3]{V} = 6.3 \times 10^{18}$ cm^{-2} stops injected electrons with start energy below 5.6 keV, i.e., we are very near a thick target at the energies where we have observed emission. Using Equation (B3) of Appendix B to obtain the low-energy cutoff value E_C that equates thermal and nonthermal energies, we obtain $E_C = 6.3$ keV. A plausible value, although flares have never been observed to go that low (partly because thermal emission usually blocks any attempts at such observations, see, e.g., Holman et al. 2003; Kontar et al. 2008). We find the total number of injected electrons in this case to be $F_{\rm tot} = 8.5 \times 10^{34}$ electrons s^{-1} above 6.3

keV. This injection rate is at least an order of magnitude below typical large flare values (Holman et al. 2003). Assuming accelerated electrons escape (which need not be the case), this rate implies the HACXS must be replenished every ≈ 40 minutes, far from the "flare number problem," where the acceleration region is estimated to be replenished sometimes as fast as every few tens of seconds (see, e.g., Miller et al. 1997).

A photon spectral index of $\gamma \approx 8$ is not very flare-like, although not unlike what Liu et al. (2008) have found in coronal sources during the impulsive phase of a flare. Smaller γ are permissible, but will decrease E_C correspondingly, in order to conserve P to the same required amount. E_C cannot be below ≈ 1 keV, the thermal temperature of the plasma: at these energies, electrons would essentially be indistinguishable from the local thermal plasma, and not contribute energy to a nonthermal beam of electrons (Emslie et al. 2003). For $E_C = 1$ keV, a $\gamma = 3.2$ nonthermal power law would conserve the injected nonthermal power and still be concealed below the thermal emission.

While it is to be noted that low-energy cutoffs below 10 keV have so far never been reliably observed, the heating of the HACXS over 12 hr purely by accelerated electrons cannot be firmly contradicted by our observations.

3.4. Connection between RHESSI Observations and UVCS Observations

There is a small overlap in time when both *RHESSI* observes the bottom of the CS (at an altitude of about 0.3 R_S), and UVCS can make a reliable temperature diagnostic of the CS at 0.7 R_S: on 2002 November 27, between 00:00 and 01:10, both *RHESSI* and UVCS sources indicate temperatures of ≈ 8 MK. If one infers that this temperature is constant between these two altitudes, one can estimate the total amount of (thermal) energy contained within this region.

Assuming a rectangular sheet with $\approx 100''$ width, ≈ 0.4 R_S length, $\approx 10^4$ km thickness (as assumed by Bemporad et al. 2006), then one gets a volume $\approx 2 \times 10^{29}$ cm^3. Assuming that the average electron density to be the geometric mean between what is found by *RHESSI* at 0.3 R_S ($\approx 10^9$ cm^{-3}) and what is found by UVCS at 0.7 R_S ($\approx 7 \times 10^7$ cm^{-3}, according to Bemporad et al. 2006), one finds a total of $\approx 6 \times 10^{37}$ electrons, for a total thermal energy content of $\approx 4 \times 10^{37}$ keV, or $\approx 6 \times 10^{28}$ erg, i.e., about 7% of the instantaneous thermal energy found in the HACXS (and about 0.1% of the total energy that must have been injected in the HACXS over 12 hr).

Hence, it is conceivable that the energy that powers the CS comes from the HACXS region, e.g., via heat conduction, and not only via magnetic reconnection in the CS. On the other hand, the fact that the HACXS starts before the CME ($\approx 13:40$ vs. $\approx 17:00$), the fact that the Bemporad (2008) nonthermal turbulent reconnection model explains well the UVCS observations, and the fact that the expelled material observed in EUV appears to flow beside the EUV loop system and the HACXS, still leaves the question open as to whether the CME/CS and the HACXS are significantly tied together.

4. SUMMARY AND CONCLUSION

UVCS observations in the wake of a CME that started around 2002 November 26 17:00 UT show hot plasma (initially well over 8 MK) at 0.7 R_S above the photosphere, for 2.3 days (at which point it had cooled down below ≈ 3.5 MK and was no longer observed). This hot plasma was interpreted as the signature of CS material.

X-ray observations during the same time interval show enhanced X-ray emissivity throughout that period, albeit at lower altitudes ($\lesssim 0.3\ R_S$). For 12 hr, *RHESSI* observes a thermal coronal source that is near the base of the CS, and, as it has at least an order of magnitude more thermal energy, it could technically provide the heat for the CS (i.e., in this scenario, reconnection, and plasma heating occur mostly near the looptops rather that in the CS). On the other hand, heat and energy transport through a turbulent environment (as is probably the CS) can be quite complex and slow (usual plasma coefficients must be replaced by effective ones: anomalous heat conductivity), and as turbulent reconnection in the CS (Bemporad 2008) explains elegantly the CS temperature, it is possible that the coronal X-ray source and EIT looptop system are only weakly related to the CS/CME.

We used novel long-accumulation imaging spectroscopy techniques to better estimate the photon spectrum and we have fitted it with an isothermal component. The *RHESSI* source temperature peaked at 10–11 MK. The emission measure of this source essentially increased during this whole 12 hr period, reaching above 5×10^{47} cm^{-3}.

We have also observed an energy versus position displacement in the emission from this HACXS, consistent with a plasma that has a Gaussian profile for its temperature distribution with altitude.

Because of the lack of observed nonthermal emission, it appears unlikely, though not impossible, that the heating in the HACXS is due to particles being accelerated in it.

APPENDIX A

THERMAL BREMSSTRAHLUNG AND EMISSION ENERGY GRADIENT

The photon flux of an isothermal plasma of temperature T and emission measure EM is given by

$$I(\varepsilon) = C_{\text{thermal}} \, \text{EM} \, \frac{1}{\varepsilon} \frac{e^{-\varepsilon/kT}}{\sqrt{kT}}, \tag{A1}$$

where k is Boltzmann's constant, ε is the observed photon energy, and the constant, $C_{\text{thermal}} = 1.54 \times 10^{-42}$ photons s^{-1} cm keV$^{1/2}$. In the following, both the emission measure EM and the temperature T will be assumed to be functions of z, the altitude above the photosphere. Hence, $I(z, \varepsilon)$ reaches a maximum along z when $\frac{dI}{dz} = 0$.

$$\frac{dI}{dz}(z, \varepsilon) = \frac{\partial \text{EM}}{\partial z} \frac{1}{\varepsilon} \frac{e^{-\varepsilon/kT}}{\sqrt{kT}} + \frac{\text{EM}}{\varepsilon} \frac{\partial}{\partial z} \left(\frac{e^{-\varepsilon/kT}}{\sqrt{kT}} \right), \tag{A2}$$

$$= \frac{\partial \text{EM}}{\partial z} \frac{1}{\varepsilon} \frac{e^{-\varepsilon/kT}}{\sqrt{kT}} + \frac{\text{EM}}{\varepsilon} \frac{\partial kT}{\partial z} \frac{\partial}{\partial kT} \left(\frac{e^{-\varepsilon/kT}}{\sqrt{kT}} \right), \tag{A3}$$

$$= \frac{\partial \text{EM}}{\partial z} \frac{1}{\varepsilon} \frac{e^{-\varepsilon/kT}}{\sqrt{kT}} + \frac{\text{EM}}{\varepsilon} \frac{\partial kT}{\partial z} \frac{e^{-\varepsilon/kT}}{(kT)^{3/2}} \left(\frac{\varepsilon}{kT} - \frac{1}{2} \right), \tag{A4}$$

$$= \frac{1}{\varepsilon} \frac{e^{-\varepsilon/kT}}{\sqrt{kT}} \left[\frac{\partial \text{EM}}{\partial z} + \frac{\text{EM}}{kT} \frac{\partial kT}{\partial z} \left(\frac{\varepsilon}{kT} - \frac{1}{2} \right) \right], \tag{A5}$$

i.e., $\frac{dI}{dz} = 0$ when:

$$\frac{1}{\text{EM}} \frac{\partial \text{EM}}{\partial z} + \frac{1}{T} \frac{\partial T}{\partial z} \left(\frac{\varepsilon}{kT} - \frac{1}{2} \right) = 0. \tag{A6}$$

Let us briefly study a few solutions that satisfy Equation (A6).

1. *Assuming $T = const$ along z.* Then $\frac{dI}{dz} = 0$ when $\frac{\partial \text{EM}}{\partial z} = 0$, i.e., EM is also constant along z. Emission at all energies is hence constant along z.
2. *Assuming EM = const along z.* Then $\frac{dI}{dz} = 0$ when $\frac{1}{T} \frac{\partial T}{\partial z} \left(\frac{\varepsilon}{kT} - \frac{1}{2} \right) = 0$. If $T(z)$ is monotonic, then this reduces to $\left(\frac{\varepsilon}{kT} - \frac{1}{2} \right) = 0$, which leads to the conclusion that not only are the higher energies emitted from regions of higher temperatures, but that these temperatures are of the order of ε. A nonmonotonic $T(z)$ can modify that behavior somewhat.
3. *Assuming exponential profiles for T and EM.*

$$T(z) = T_0 \, e^{(z-z_0)/H_T}, \tag{A7}$$

$$\text{EM}(z) = \text{EM}_0 \, e^{-(z-z_0)/H_{\text{EM}}}, \tag{A8}$$

where $T(z)$ and $\text{EM}(z)$ are the temperatures and differential emission measures along (a loop) path z. T_0 and EM_0 are constants. H_T and H_{EM} are scale heights. The peak of emissions at energy ε, located at z are expected to follow the functional relation:

$$z - z_0 = H_T \ln \left(\frac{\varepsilon}{k T_0 \left(1/2 + H_T/H_{\text{EM}} \right)} \right). \tag{A9}$$

These profiles diverge, and are of course globally unphysical. At best, this model can only apply locally.

4. *Assuming Gaussian profile for T and exponential for EM.*

$$T(z) = T_0 \, e^{-((z-z_0)/H_T)^2}, \tag{A10}$$

$$\text{EM}(z) = \text{EM}_0 \, e^{-(z-z_0)/H_{\text{EM}}}, \tag{A11}$$

which leads to a slightly more complicated functional relationship:

$$\varepsilon = \frac{k T_0}{2} e^{-\left(\frac{z-z_0}{H_T} \right)^2} \left(1 - \frac{H_T^2}{H_{\text{EM}}} \frac{1}{z - z_0} \right). \tag{A12}$$

APPENDIX B

NONTHERMAL EMISSION FORMULAE

B.1. Thick-target Assumption

The nonthermal photon power law produced by the power-law distribution of electrons that produced it can be related by the following formula (Brown 1971; Hudson 1972):

$$\Phi_{\text{thick}}(\varepsilon) = C_{\text{thick}}(\delta) \frac{F_{\text{tot}}}{(\delta - 2)} E_c^{\delta-1} \varepsilon^{1-\delta}, \tag{B1}$$

$$= C_{\text{thick}}(\delta) \frac{P_{\text{nth}}}{(\delta - 1)} E_c^{\delta-2} \varepsilon^{1-\delta}, \tag{B2}$$

where $\Phi_{\text{thick}}(\varepsilon)$ is the photon flux at 1 AU, for photon energy ε (in keV), in photons s^{-1} cm^{-2} keV^{-1}. $C_{\text{thick}}(\delta) = 1.5 \times 10^{-34} B(\delta - 2, 1/2)$, B is the Beta function, F_{tot} is the total number of electrons per second above the cutoff energy E_c, δ is the injected electron spectral index, and is equal to $\gamma + 1$, where γ is the photon power-law spectral index. $P_{\text{nth}} = \frac{\delta-1}{\delta-2} E_c F_{\text{tot}}$ the nonthermal power in accelerated electrons, in keV s^{-1}.

Equation (B2) can also be rewritten as

$$E_c = \left(\frac{6.7 \times 10^{33}}{B(\gamma - 1, 1/2)} \gamma \, \varepsilon^{\gamma} \, \frac{\Phi(\varepsilon)}{P_{\text{nth}}} \right)^{\frac{1}{\gamma-1}}. \quad \text{(B3)}$$

B.2. Thin-target Assumption

Using the same notations as in the preceding paragraph:

$$\Phi_{\text{thin}}(\varepsilon) = C_{\text{thin}}(\delta) N (\delta - 1) F_{\text{tot}} E_c^{\delta-1} \varepsilon^{-1-\delta}, \quad \text{(B4)}$$

$$= C_{\text{thin}}(\delta) N P_{\text{nth}} E_c^{\delta-2} \varepsilon^{-(\delta+1)}. \quad \text{(B5)}$$

N is the column density traversed by the electrons (cm^{-2}), $C_{\text{thin}}(\delta) = 4.05 \times 10^{-52} \frac{B(\delta,1/2)}{\delta}$, $\delta = \gamma - 1$. This formula is valid when $\varepsilon_{\text{keV}} \gg \left(\frac{N}{2 \times 10^{17} \text{ cm}^{-2}} \right)^{1/2}$.

Equation (B5) can be rewritten as

$$E_c = \left(\frac{2.5 \times 10^{51}}{B(\gamma - 1, 1/2)} \frac{\gamma - 1}{\gamma - 3} \varepsilon^{\gamma} \frac{\Phi(\varepsilon)}{N P_{\text{nth}}} \right)^{\frac{1}{\gamma-3}}. \quad \text{(B6)}$$

REFERENCES

Aschwanden, M. J. 2004, Physics of the Solar Corona. An Introduction (Chichester: Praxis Publishing Ltd.; New York: Springer)
Bemporad, A. 2008, ApJ, 689, 572
Bemporad, A., Poletto, G., Suess, S. T., Ko, Y.-K., Schwadron, N. A., Elliott, H. A., & Raymond, J. C. 2006, ApJ, 638, 1110
Brown, J. C. 1971, Sol. Phys., 18, 489
Brown, J. C., Aschwanden, M. J., & Kontar, E. P. 2002, Sol. Phys., 210, 373
Brueckner, G. E., et al. 1995, Sol. Phys., 162, 357
Ciaravella, A., & Raymond, J. C. 2008, ApJ, 686, 1372
Ciaravella, A., Raymond, J. C., Li, J., Reiser, P., Gardner, L. D., Ko, Y.-K., & Fineschi, S. 2002, ApJ, 575, 1116
Delaboudinière, J.-P., et al. 1995, Sol. Phys., 162, 291
Emslie, A. G., Kontar, E. P., Krucker, S., & Lin, R. P. 2003, ApJ, 595, L107
Gallagher, P. T., Dennis, B. R., Krucker, S., Schwartz, R. A., & Tolbert, A. K. 2002, Sol. Phys., 210, 341
Holman, G. D., Sui, L., Schwartz, R. A., & Emslie, A. G. 2003, ApJ, 595, L97
Hudson, H. S. 1972, Sol. Phys., 24, 414
Hurford, G. J., et al. 2002, Sol. Phys., 210, 61
Ko, Y.-K., Raymond, J. C., Lin, J., Lawrence, G., Li, J., & Fludra, A. 2003, ApJ, 594, 1068
Kohl, J. L., et al. 1995, Sol. Phys., 162, 313
Kontar, E. P., Dickson, E., & Kašparová, J. 2008, Sol. Phys., 252, 139
Kopp, R. A., & Pneuman, G. W. 1976, Sol. Phys., 50, 85
Lin, J., & Forbes, T. G. 2000, J. Geophys. Res., 105, 2375
Lin, J., Ko, Y.-K., Sui, L., Raymond, J. C., Stenborg, G. A., Jiang, Y., Zhao, S., & Mancuso, S. 2005, ApJ, 622, 1251
Lin, R. P., et al. 2002, Sol. Phys., 210, 3
Liu, W., Petrosian, V., Dennis, B. R., & Jiang, Y. W. 2008, ApJ, 676, 704
Miller, J. A., et al. 1997, J. Geophys. Res., 102, 14631
Raymond, J. C., Ciaravella, A., Dobrzycka, D., Strachan, L., Ko, Y.-K., Uzzo, M., & Raouafi, N.-E. 2003, ApJ, 597, 1106
Saint-Hilaire, P., Krucker, S., Christe, S., & Lin, R. P. 2009, ApJ, 696, 941
Schmahl, E. J., & Hurford, G. J. 2003, Adv. Space Res., 32, 2477
Sui, L., & Holman, G. D. 2003, ApJ, 596, L251
Svestka, Z. 1987, Sol. Phys., 108, 411